

A Cost-Effective Slag-based Mix Activated with Soda Ash and Hydrated Lime: A Pilot Study

Jayashree Sengupta¹, Nirjhar Dhang², and Arghya Deb³

¹Research Scholar, Dept. of Civil Engineering, Indian Institute of Technology, Kharagpur, West Bengal 721302, India. Email: jaish.sengupta@iitkgp.ac.in.

²Professor, Dept. of Civil Engineering, Indian Institute of Technology, Kharagpur, West Bengal 721302, India.

³Professor, Dept. of Civil Engineering, Indian Institute of Technology, Kharagpur, West Bengal 721302, India.

Abstract

This study investigates the cost-effective binder material of silica fume blended slag mix using industry grade soda ash and hydrated lime as solid activators. The study followed a "just add water" methodology, observing paste rheology and strength development. Microstructural analysis and TGA-DTA studies were conducted to validate the results. A side-by-side comparison was conducted with other mixing procedures. The study found that using pre-mixed analytical grade Na_2CO_3 in water can cost up to 60% more than using a mixture activated by NaOH pellets. Using industrial-grade chemicals could save 94.5 percent of the budget. For a 10% SF addition and a 10% targeted NaOH content at a w/s ratio of 0.45, the mixes showed the highest strength development and commendable rheology. The mix demonstrated 35.1 MPa after 28 days and 41.33 MPa after 120 days, making it suitable for use as a structural material. The presence of magnesian calcite, magnesite, and hydrotalcite was detected in the XRD analyses. SEM images showed a denser microstructure developed at 28 days. The TG-DT analysis provided insights into phase transitions and bound water associated with hydration products. The higher strength was attributed to calcite transitioning into magnesian calcite and portlandite supplanting CNASH and CSH.

Keywords: soda ash, hydrated lime, alkali-activated, compressive strength, rheology, thermogravimetric analysis

1. Introduction

It is widely acknowledged that natural aluminosilicates can be combined with common limestones to create durable building materials. Roman concrete, which is still regarded as an architectural marvel, is one such example (Jackson et al., 2017; Seymour et al., 2022). Following the same grounds, alkali activation of industrial or agricultural by-products, is a recent technological advancement that is valued in order to create a "greener" binder (Provis, 2018; Shi et al., 2011). These "alkali-activated binders" produce concrete that is similar to that made with conventional cement. These exhibit different microstructural compositions based on the raw materials used. Thus, alkali-activation not only helps to value industrial and agricultural wastes but also reduces or even eliminates the need for cement. "No cement" would lower airborne carbon dioxide emissions (Flower and Sanjayan, 2007; Teh et al., 2017; Wu et al., 2018). Precursors are non-reactive aluminosilicates that gain binding properties when exposed to alkalis. When alkalis are added, the aluminosilicates disintegrate, releasing tetrahedral monomers. The excess oxygen is shared between the metal ion and alumina, creating a polymeric gel with stronger bonds. Alkalis are typically sodium or potassium-based, with silicate-based solutions (Hardjito and Rangan, 2005). Alkali-earth metals like calcium and magnesium can enhance mechanical strength and durability (Yip et al., 2005).

Despite the benefits listed above, alkali activation has not yet been incorporated into routine concrete practice. This is primarily due to- (i) the need for trained supervision when using alkalis in solution form (ii) the fact that alkali solutions are highly skin-corrosive and can result in first-degree burns if handled improperly (iii) the use of silicates increases CO₂ emissions and (iv) the cost of the alkalis and the corresponding storage requirements, which adds to the budgetary burden of construction. One-part mixing is employed to get around the first two limitations, which make use of solid activators and a "just-add-water" strategy (Luukkonen et al., 2018). When activators are added as solids, the chemistry changes slightly. Before the aluminosilicate dissociations, the activators are hydrolyzed. Consequently, in one-part mixing, specific factors have impacted the dissolution. Like the choice and reactivity of the activator being used, as well as the amount of water. Both of which, when combined, should aim an increase in strength. Hence in the present study, it is aimed that the cost of alkali activation did not outweigh the benefits.

Previous studies have explored alternative activators made from silica-rich wastes, such as rice husk ash (RHA), ground waste glass (WG), and silica fume (SF), to replace sodium silicate solutions. These activators were designed by dissolving waste products in NaOH or KOH concentrated solutions. The RHA-based activator showed similar strength development as sodium silicate (Handayani et al., 2022), but higher RHA content may affect the mix's flow characteristics (Athira and Bahurudeen, 2022). The WG-NaOH activated mix had higher compressive strength than a silicate activated mix. Silica fume was more effective than RHA (Vigneshwari et al., 2018), as it benefited from its filling action, creating more calcium silicate hydrates (Kang et al., 2019; Nežerka et al., 2019; Rostami and Behfarnia, 2017), increasing strength and durability. However, higher amounts of silica fume resulted in a reduction in strength (Cheah et al., 2019) and increased volume of large capillary pores (Li et al. 2022). The optimal SF amount was 10%. Sugarcane straw ashes was mixed in NaOH and pre-conditioned for 24 hours to obtain a strength over 50 MPa (Moraes et al., 2017). Pastes made from olive biomass ash and GGBFS showed a 28-day mechanical strength between 33 to 18 MPa (Alonso et al., 2019). However, caustic alkalis were still used in the process, putting a strain on budgets and posing a problem with handling caustic solutions. Red mud has been used as an alternative to NaOH for activating fly ash mixtures (Choo et al., 2016), with 60% red mud being equivalent to 3-4% of NaOH activated. However, region-specific availability of waste is a constraint. Na_2CO_3 and Na_2SO_4 are milder and cheaper alternatives, but they are not strong enough to raise the pH of the system to maintain dissolution mechanisms. Na_2CO_3 has the potential to be used as an activator when combined with other additives, potentially speeding up the reaction (Adesina, 2020). (Akturk et al., 2019) reported an 28-day strength development ranging between 28-45 MPa for different combination of Na_2CO_3 - $\text{Ca}(\text{OH})_2$ - NaOH. A combination of analytical grades is more expensive than NaOH alone. Therefore, it remains to be recognized as a beneficial, user-friendly, easily available, and cost-effective activator for one-part mixing.

Soda ash, the industrial grade sodium carbonate, is a extensively used chemical in glass, detergent, paper, and chemical manufacturing sectors. It is used to treat water and as a food additive. It is widely used globally and is easily accessible. Industrial grade hydrated lime is also used in water and waste treatment, and construction processes. It is available in purity levels ranging from 75% to 96%, depending on the CaO content. Studies have

shown that analytical grade chemicals improve mix properties, but less pure industrial grade chemicals like soda ash and hydrated lime have not been investigated. The industrial grade chemicals are less expensive given the less purity than analytical counterparts. These activators could thus be used as an alternative activator for strength development in structural applications. Mechano-chemical processing of the raw materials can result in early strength development, but pre-processing could affect cost effectiveness. Therefore, this study adopted a dry direct mixing of activators and precursors without any pre-processing like in (Kearsley et al., 2015). Ambient curing is adopted due to its energy-intensive nature and sustainability standpoint.

The present study thus involved mixing the chemicals directly in solid form to the precursors. The effect on fresh and hardened properties are observed. Mixes activated by NaOH pellets pre-mixed in water, are also included for comparison purposes only. The rheological properties and the strength development are observed for the different types of mixing techniques. Microstructural characterization of selected mortar samples is also performed to support the obtained results of the one-part mixes. The same is not done for the NaOH and pre-mixed activator samples because it is outside the scope of the current study. Finally, the major contributions of the study are summarized. It is anticipated that this alkali-activated slag-based binder would meet the requirements of the construction industry.

2. Research Significance

The goal of the current study is to demonstrate the effectiveness of using industrial grade hydrated lime and soda ash as solid activators to alkali-activate a mixture of slag and silica fume. Different mixing techniques were used, and their influence on the corresponding fresh and hardened properties was examined. Although it was demonstrated in a prior study (Kearsley et al., 2015) that a designed NaOH mix, activated by reagent grade chemicals, reached its maximum strength at 6%, the current study did not give the optimal percentage in the same range. It was obvious that the mixing technique and the quality of the activators used, namely purity, had a significant impact on the fresh and hardened properties of the mixes. Additionally, Table 1 shows a noteworthy cost difference when using industry grade chemicals. Using pre-mixed analytical grade Na_2CO_3 in water can cost up to 60% more than using a mixture activated

by NaOH pellets. On the other hand, using industrial-grade chemicals could cut down the costs by 91%. When compared to analytical Na₂CO₃ counterparts, it saves 94.5% of the budget.

Table 1: Cost comparisons for analytical and industrial grades chemicals for 10% NaOH equivalents of activators for 1m³ of mix

Industrial grade soda ash (as solid or pre-mixed in water) and hydrated lime (as solid) (INR/m ³)	Analytical grade NaOH pellets in water (INR/m ³)	Analytical grade Na ₂ CO ₃ and Ca(OH) ₂ added in powder form (INR/m ³)	
3428.49	39426.60	63115.13	
Costing Schedule			
Types	Measured as	Cost	Ref
Analytical grade NaOH	INR per kg	690.00	(Sodium Hydroxide CAS 1310-73-2 / 106462, n.d.)
Analytical grade Na ₂ CO ₃	INR per kg	610.00	(Sodium Carbonate CAS 497-19-8 / 106392, n.d.)
Analytical grade Ca(OH) ₂	INR per kg	320.00	(Calcium Hydroxide CAS 1305-62-0 / 102047, n.d.)
Industrial grade Soda Ash	INR per kg	35.50	(Price List for Soda Ash, n.d.)
Industrial grade Hydrated Lime	INR per kg	14.00	(Hydrated Lime - Shreeram Chemical Industries, n.d.)

3. Material and Experimental Methods

3.1. Material Characterization

Ground granulated blast furnace slag (GGBFS) from Rashmi Cement Limited, West Bengal, India was used as the aluminosilicate precursor. Powdered industrial grade hydrated lime (HL) and soda ash were obtained locally from Shreeram Chemicals Kolkata. The XRD profiles of the activators are shown in Figure 1 along with a quantification of the oxides that are present, defending the lower purity of the industrial grade chemicals. Silica fume (SF) was obtained from Walter Enterprises. Table 2 lists the chemical compositions of materials for alkali activation. The modulus of basicity (B) of GGBFS is determined by the ratio of basic oxides to acidic oxides. The slag used in this study has a B = 1.14, hence basic, making it suitable for alkali activation.

Table 2: Chemical properties of the precursor materials

	CaO	SiO ₂	Al ₂ O ₃	MgO	MnO	K ₂ O	Na ₂ O	Fe ₂ O ₃	TiO ₂	P ₂ O ₅	SO ₃	LOI
GGBFS	43.78	32.08	11.20	5.82	0.84	0.42	0.03	0.75	0.87	1.33	1.65	2.74
SF	3.81	84.12	0.15	1.43	1.15	2.70	0.02	2.64	0.40	0.72	0.33	3.41

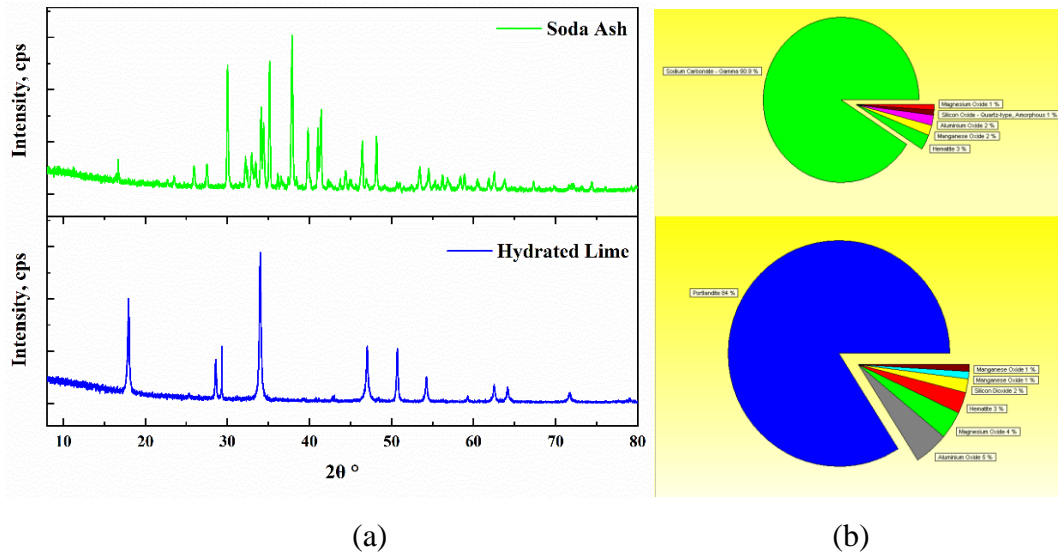


Figure 1: (a) The XRD profile of the activators (b) quantification of the oxide components of the activators.

3.2. Mix Proportions

Mortar samples were prepared using proportions shown in Table 3, and slag was replaced with silica fume at 10% and 20%. The target amount of NaOH is expected to form when hydrated lime and soda ash are mixed, avoiding unreacted sodium and efflorescence (Ren et al., 2021). For example, for 10% NaOH to form, 9.25% ($74/80 \times 10\%$) of hydrated lime and 13.25% ($106/80 \times 10\%$) of soda ash is required. The solid activators (HL + SA) are set aside as a percentage of the aluminosilicate material and additive. Real-time HL addition increases water demand, but excessive water addition may lower pH and impede ionic dissolution. A water/solids ratio of 0.45 is used to facilitate the reaction while meeting water demand. A schematic diagram of the mixing process is shown in Figure 2.

The binder-sand ratio was maintained at 1:3, and standard sand (IS 650-1966 and ASTM C109) was used for casting. The mix nomenclature includes SF10NH6, which represents 10% silica fume and 6% NaOH. For comparison of strength development, control mixtures (suffixed with C) were also tested, activated with analytical grades of solid NaOH pellets pre-mixed in water and is denoted as shown in the Table 3. Simultaneously, mortar sample were also tested with industrial grades of soda ash pre-mixed with water (suffixed with PM) and hydrated lime added in powdered form, for similar percentages of selected mixes. All mixing was carried out at room temperature.

Table 3: Mix proportion of mortars with aggregate: binder as 3:1.

Mix type	Mix ID	Binder (A)		Activators (B)		
		SF %	GGBFS %	(Targeted) NaOH %	Hydrated Lime HL %	Soda Ash SA %
Soda ash and hydrated lime added in solid form	SF10NH6	10	90			
	SF20NH6	20	80	6	5.55	7.95
	SF10NH8	10	90			
	SF20NH8	20	80	8	7.41	10.59
	SF10NH10	10	90			
	SF20NH10	20	80	10	9.26	13.25
	SF10NH12	10	90			
	SF20NH12	20	80	12	11.11	15.90
Control NaOH solution	SF10NH8_C	10	90	8	-	-
	SF20NH8_C	20	80			
	SF10NH10_C	10	90	10	-	-
	SF20NH10_C	20	80			
Pre-mixed soda ash in water	SF10NH8_PM	10	90	-	7.41	10.59
	SF20NH8_PM	20	80			
	SF10NH10_PM	10	90	-	9.26	13.25
	SF20NH10_PM	20	80			

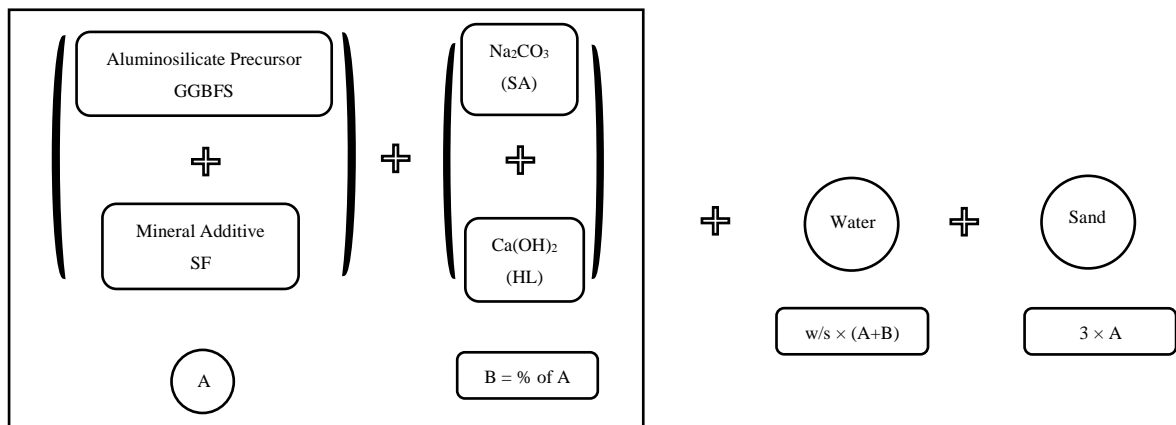


The ratio of molar mass of $\text{Ca}(\text{OH})_2$ to molar mass of 2NaOH is 74/80 and ratio of molar mass of Na_2CO_3 to molar mass of 2NaOH is 106/80.

SF10NH6_C represents 10% of silica fume and 6% of NaOH solution

SF10NH6_PM represents 10% of silica fume and 6% of pre-mixed Na_2CO_3 in water

SF10NH6 represents 10% of silica fume and 6% of equivalent NaOH resulting from the corresponding HL and SA reactions



One-part solid alkali activated binder

Figure 2: Mixing sequence of the mortar specimens

3.3. Experimental Methods and Analytical Techniques

The study used an Anton Paar MCR 302 rheometer to conduct rheological tests on cement pastes. The mixtures were tested three times, with a constant temperature of $32 \pm 0.5^\circ\text{C}$. The rheological shearing protocol involved initial pre-shearing at 100 s^{-1} for 30 s to bring the paste to a steady state, followed by a 45-second rest period, and stepped ramps with different shear rates, varying from 0-100-0 s^{-1} , with each shear rate maintained for 20 second. The flow curve was determined from the up and down shear rate stepped ramps to assess the rheological properties. The Modified Bingham (MB) model ($\tau = \tau_0 + \mu_p \dot{\gamma} + C\dot{\gamma}^2$) was used to assess yield stress values. A good linear fit ($R^2 > 0.95$) was achieved, with the MB model relating shear stress (τ) to shear rate ($\dot{\gamma}$), yield stress (τ_0), and plastic viscosity (μ_p). The regression constant was C.

The mortar samples were cast in 70.6 mm cubic moulds as per IS 4031-6: 1988 and ASTM C109. The solid binder was dry mixed with sand thoroughly for one minute. The water was then added and the blend was mixed for two minutes in a Hobart mixer. The mortar was then placed in the mould on a table of a vibrating machine. The mortar was prodded 20 times in two layers to prevent honeycombing and voids. 16 mixtures were cast, with 9 replicas each. Samples were demoulded after 24 hours, cured at ambient temperature and humidity, and tested at 7, 28, and 120 days. Compressive strengths were determined using a Tinius Olsen Model 120 hydraulic Super 'L' universal testing machine with a 60-ton load capacity.

After the samples were tested for compressive strength, powdered mortar pieces were collected. The samples were dipped in acetone for 45 minutes and then air-dried for 5 minutes. The air-dried samples were then dried in an oven for 2 hours at 60°C . The samples are then taken and kept in a vacuum desiccator until testing for XRD, SEM, and TGA. The hardened samples were analyzed for chemical composition using micrographs and XRD. Samples with highest compressive strength underwent microstructural, XRD, and thermal analysis. Microstructural analysis was performed on gold coated samples using a field emission-gun scanning electron microscope and energy dispersive spectrometer (SEM-EDS, ZEISS Merlin Scanning Electron Microscope with Oxford EDS Detector). EDS analyses were performed on 20 random points per sample to determine molar ratios. Hydrated products were identified and quantified using XRD.

Samples were prepared at 7 and 28 days and crystalline phases quantified using X'PertPRO PANalytical software. DTA-TGA was conducted using a Pyris diamond thermal analyzer, collecting powdered mortar samples from compressive strength tests. The mortar sample was heated from 27°C to 900°C, dissociating and releasing hygroscopic water and chemically bound water. The deformation process was estimated using a TG balance with a 0.1 mg accuracy.

4. Results and Discussions

4.1. Paste Rheology

Figure 3 shows the yield stress and the plastic viscosity of the different pastes. With an increase in the targeted percentage of NaOH, both the yield stress and the plastic viscosity were reduced. However, additions above 10% increased the yield stress, as shown in Figure 3. Although previous studies demonstrated the advantages of using silica fume, as the ball bearing effect reduced yield stress and improved mobility; the addition of silica fume here led to an increase in yield stress, due to the finer particle size. Figure 4 illustrates how the yield stress and plastic viscosity change with different w/s ratios. The yield stress was significantly raised for silica fume concentrations of 20%. This is due to the higher water demand imposed by a finer SF. Although, a simultaneous increase in the targeted NaOH% lowered the yield stress value, resulting from a higher dissolution of the slag particles. In case of the SF10 samples, the yield stress followed an order $w/s = 0.50 > 0.55 > 0.45$ (Figure 4). However, the plastic viscosity followed $w/s = 0.45 > 0.50 > 0.55$. This means that increasing the w/s ratio demonstrated a lower initial flow resistance, but once the material begins to deform, it demonstrated a higher internal friction, resulting in a higher viscosity. A higher inter-particle friction indicated that the particles were bound more tightly, restricting the flow. This in turn resulted in a denser microstructure. Which was why, the viscosity for $w/s=0.45$ was high even if the yield stress was much lower, indicative of an ordered microstructure to have formed. The strength and TGA results, which will be covered later, also confirmed this. Similar to this, at $w/s=0.55$, a higher yield stress was seen, and an immediate drop in viscosity indicated the otherwise. It is to be noted that all samples showed shear thinning behaviour ($C < 0$).

The soda ash acted more as an accelerator when added in the form of a pre-mixed solution, and a quick set was observed for all pre-mixed (PM) mixes. The dissolution was subdued

by the readily available CO_3^{2-} ions in solution form. According to earlier studies, the presence of carbonate ions caused the medium to become more acidic and produce alkaline carbonates, which reduced the degree of reaction (Garcia-Lodeiro et al., 2015). On the other hand, when added in solid form, the soda ash first reacted with the hydrated lime to form NaOH which in turn potentially react with slag particles and hence lowering the yield stress. Also, in comparison to a soda ash solution of the same weight, anhydrous soda ash typically contained a higher concentration of alkali. Thus, the formation of the hydration product was masked down by the reduced alkali concentration in the PM mixes. In the control mixes, on the other hand, the higher alkalinity of the NaOH solution itself raised the dissolution rate of the slag. Both the plastic viscosity and the yield stress were observed to have significantly decreased. The reduced yield stresses made it clear that the gel structures formed unimpeded. This in turn made the mixture more fluid.

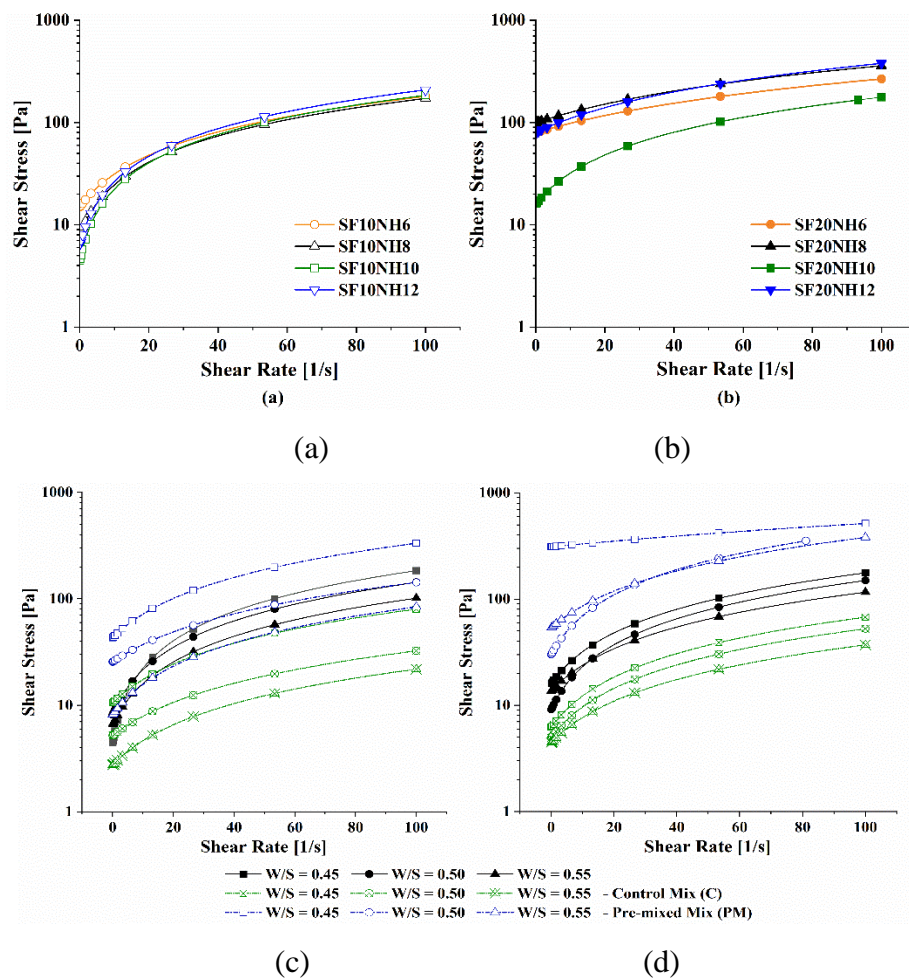


Figure 3: Shear stress variation of different one-part pastes with the shear rate of- (a) SF10 mixes (b) SF20 mixes; (c) SF10NH10 and (d) SF20NH10 at different w/s ratios with respect to different mixing procedures.

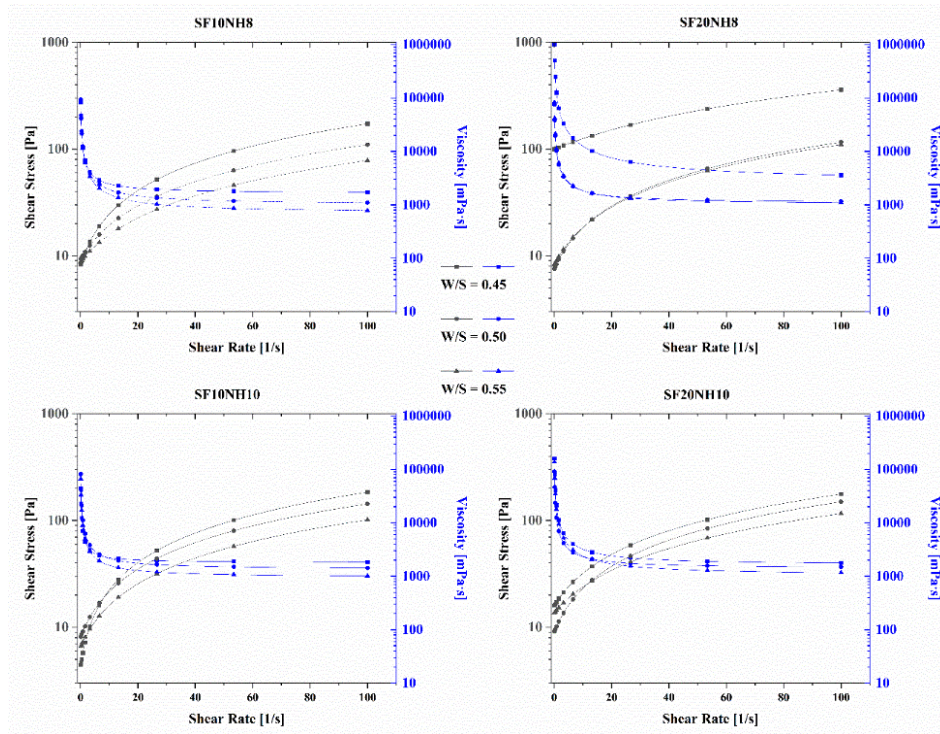


Figure 4: Shear stress and viscosity variation of different one-part pastes at different w/s ratio.

4.2. Compressive strength

Figure 5 depicts the strength development of the samples after 7, 28, and 120 days of curing. SF10NH8, SF20NH8, SF10NH10, and SF20NH10 have higher initial strengths. The 120-day strength of all samples reached a maximum in the same range for both 10% and 20% SF addition. However, the rate of strength gain varied significantly depending on the percentage of silica fume added. This indicated the possibility of a secondary reaction. The initial strength was observed to be more than 20 MPa for a targeted NaOH percentage greater than 6%, while the later-age strength was more than 30 MPa, establishing the competency of the mixes for structural application. SF10NH8, SF20NH8, SF10NH10, and SF20NH10 demonstrated the best strength development, with the 28-day strength of 35.1 MPa and the 120-days strength of 41.33 MPa for SF10NH10. All the mixes were also prepared for water-to-solids (w/s) ratios of 0.5 and 0.55 using a mixing process similar to that described in section 3.2. Figure 6 depicts the strength development of the mixes for other w/s ratios. The compressive strength was reduced as the w/s ratio increased. This was because a higher w/b ratio tended to dilute the system by affecting the H_2O/Na_2O ratio. As a result, ion dissolution was hampered, resulting in a decrease in strength.

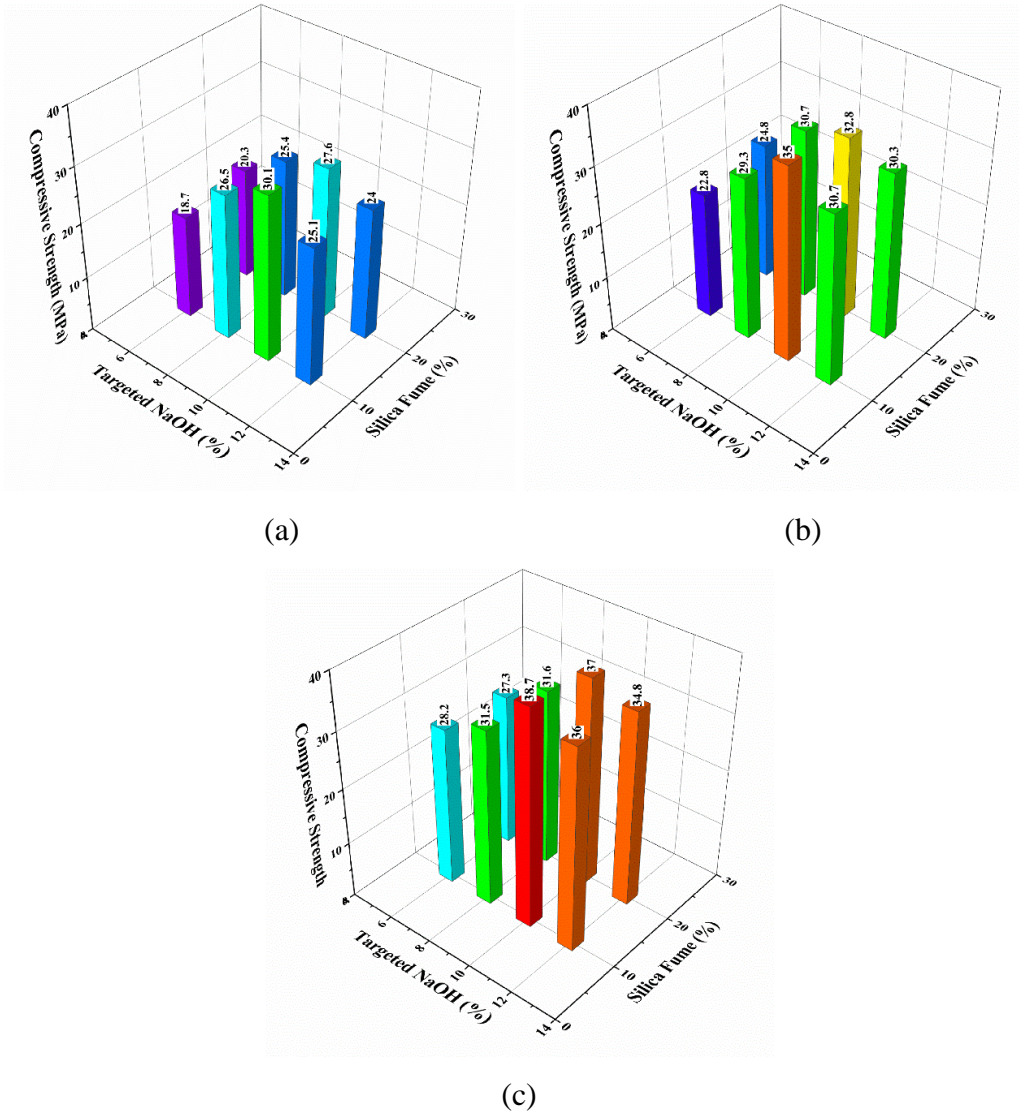


Figure 5: Strength development of various one-part mixes at different ages of curing in sequence of 7, 28 and 120 days.

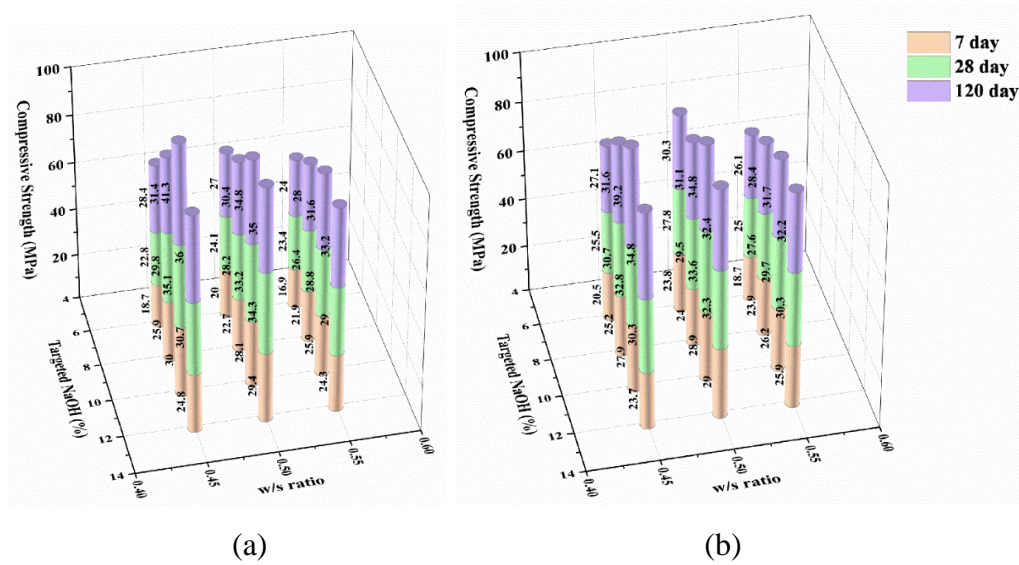


Figure 6: Strength variation with w/s ratios of (a) 10% SF and (b) 20% SF addition

The simultaneous strength development of a NaOH solution activated (control) mix was also tested. The initial strength was noticeably lower than that of the solid activator mixed samples, as shown in Figure 7. The initial strength was reduced as the sodium content was increased. However, the later age strength improved considerably. The rate of strength gain was not systematic for the samples, though. This could be attributed to the competition between the Na^+ and Ca^{+2} ions, due to Lewis acidity, hindering the reaction. In addition, a pre-mixed soda-ash solution was used to activate a GGBFS-SF-calcium hydroxide mix, and the initial strength development was high, in line with the previous studies (Akturk et al., 2019). This could be because the system was activated solely by soda ash, while hydrated lime acted as an additive (Bernal et al., 2014) reported slow activation by Na_2CO_3 , where the primary reaction formed gaylussite, which then formed calcite and hydrotalcite. The hydrated lime mostly balanced off the CO_3^{-2} ions in the pore solution in the pre-mixed soda-ash solution blends. A higher 28-day strength was observed for the pre-mixed soda ash mixes. In all cases, though, 10% SF and 10% NaOH (direct as well as equivalent) showed the maximum strength development. The same set of raw materials were the subject of an investigation by (Kearsley et al., 2015), who reported compressive strengths of 45–50 MPa at 28 days and 6% alkali concentration. The mechano-chemical processing of the raw materials did, however, help with the development of strength. It also demonstrated clearly that high strength could be achieved by the analytical chemicals at a much lower percentage. The GGBFS used in the above study was reported to be neutral, it didn't specifically state the chemical grade, and the mix design was different, so it couldn't be used as a benchmark for comparing the strength development in the present study, by the analytical grades. In order to validate any differences, additional tests were conducted to compare mixtures with analytical grade Na_2CO_3 and $\text{Ca}(\text{OH})_2$ complements. Comparing the analytical grade chemical activated mix to the industrial grade complements, the strength was higher for the former. The variation in the strength development of the selected mixes are shown in Figure 7. The strength of the one-part mix was higher than the mixes activated by the NaOH solution, and lower than the pre-mixed soda ash mix. Although a targeted NaOH incorporation resulted in a simultaneous CaCO_3 existence, it contributed to the strength enhancement. This is consistent with the findings of (Ma et al., 2019), who found calcite formation to be a stable polymerization product in a Na_2CO_3 activated fly ash mixture. CaCO_3 filling was reported beneficial with reduced porosity (Wang et al., 2018). Additionally, after 120 days of curing, there was a subsequent improvement.

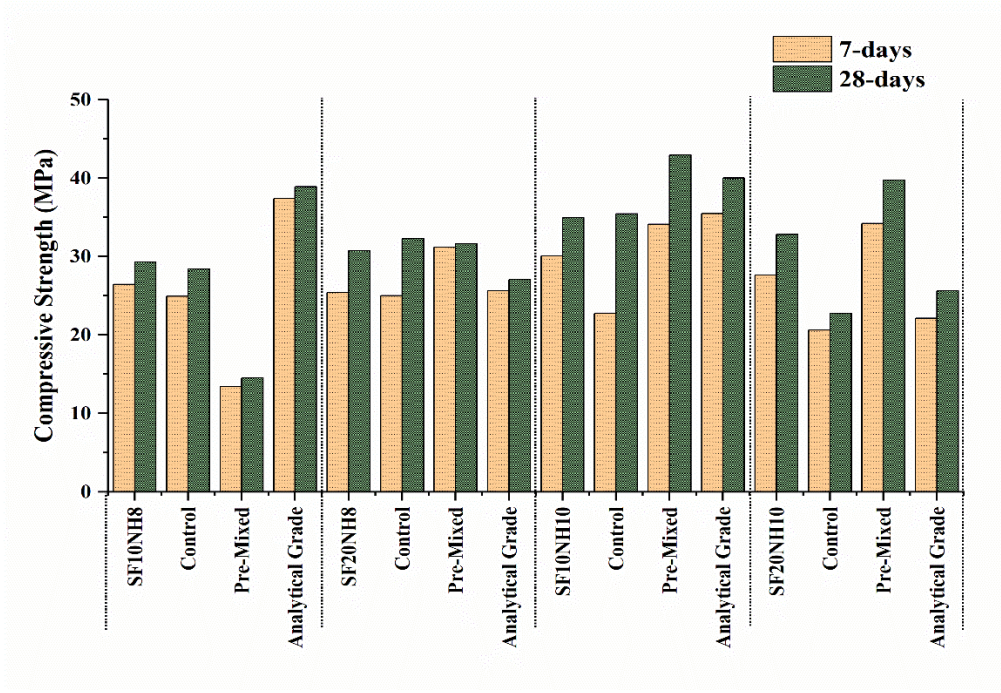


Figure 7: Strength comparison of the mixes, the equivalent Control NaOH solution activated mix and the Pre-mixed soda ash in water activated mix at w/b ratios of 0.45.

4.3. Phase Analysis through XRD

The mixes with the highest strength were chosen for microstructural analysis. As a result, SF10NH8, SF20NH8, SF10NH10, and SF20NH10 were chosen. The phases formed are identified using X'Pert Highscore Plus v3.0. Figure 8 depicts the main reaction products. N-A-S-H (Zeolite X, Ca- exchanged, #98-001-2576), C-N-A-S-H (Zeolite A, #98-002-2602), calcite (#00-005-0586), mineral portlandite (#98-005-8830), brucite (#98-003-5306), gibbsite (#98-012-3163), and quartz (#00-033-1161) were detected. The degree of irregularity in the pattern could be interpreted as it diffracted the X-rays. In an amorphous state, the diffraction of X-rays resulted in broadly diffused halo rather than sharp diffraction peaks. The broad and amorphous convexity, centered at around 27–29° (2θ) was the characteristic peaks of amorphous gels including zeolitic gels and calcium silicate hydrate gels, typical of the diffraction pattern of alkali-activated materials (Alonso and Palomo, 2001; Alventosa and White, 2021; Li et al., 2019). The more convex, the more the strength. The alkali activation reaction and hydrate reaction occurred simultaneously, with quartz and calcite being the main peaks in XRD. Calcite formation was caused by the initial cation exchange reaction between soda ash and hydrated lime, resulting in sodium hydroxide and calcium carbonate. Calcium carbonate prevents ettringite formation (Jiao et al., 2018). The intensity of calcite peaks decreased at 28 days due to

the simultaneous formation of magnesites and magnesian calcites. Brucites were detected in the 7-day sample but not in the 28-day sample, likely reacted with calcite to form portlandite and magnesite. The presence of C-N-A-S-H was absent in the 7-day sample. Gaylussite (Abdalqader et al., 2016) was not found in the XRD.

Portlandite diffraction peaks were observed in all samples, but their intensity dropped significantly at 28 days. The presence of portlandite (mineral) could be a secondary reaction product, as the formation of calcite ensured the formation of sodium hydroxide. Tobermorite 14 A, zeolite X (Ca- exchanged and Na- exchanged) were identified in all samples, with no obvious strong peaks indicating amorphous nature. Specific trona peaks in SF20NH10 were observed, indicating the presence of unreacted sodium carbonate. All samples exhibited zeolite A (C-N-A-S-H) at 28-days. Thaumascite peaks (98-007-9112) were also detected in the 28-day samples. Hydrotalcite characteristic peaks (98-000-6182) were also observed in SF10NH8 at 7 days, but not in other samples. However, a hydrotalcite peak was observed in all 28-day samples with a d-spacing of 1.25 Å and 75.78(2). Brucite peaks were also detected in all samples, with the intensity decreasing or disappearing after 28 days.

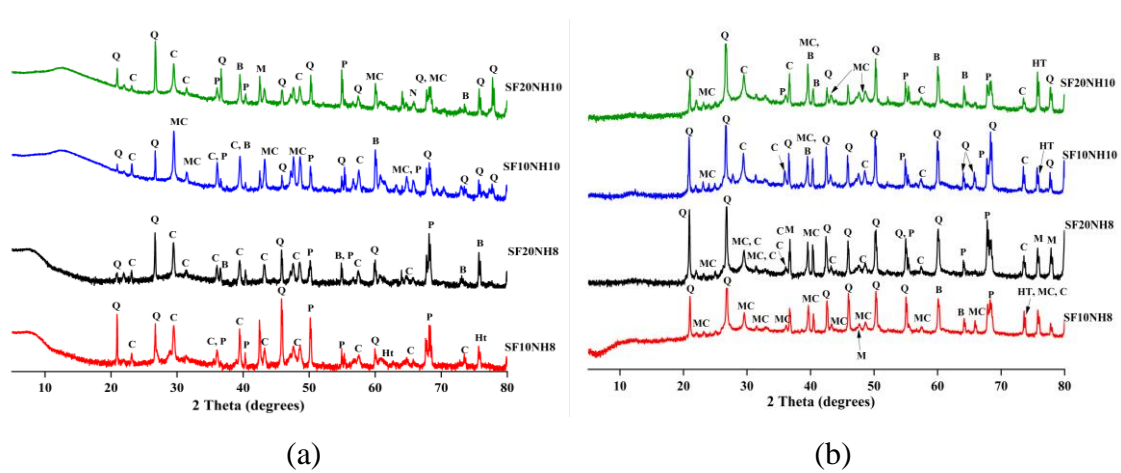


Figure 8: XRD of the mortar samples at (a) 7 days (b) 28 days. Q= Quartz; P= Portlandite; C= Calcite; B= Brucite; M= Magnesite; MC= Magnesian Calcite; HT= Hydrotalcite

4.4. Microstructural Characterization

Scanning electron micrographs (Figure 9 and Figure 10) show cubic crystal formations in 7-day samples, with scattered micro-cracks. Calcite crystallized during initial ion

exchange reactions, and SF20NH10 had a calcite-rich microstructure after 7 days of curing. XRD revealed NaOH presence, confirming unreacted aluminosilicates. After 28 days, microstructures developed into dense and compact systems, consistent with strength development results.

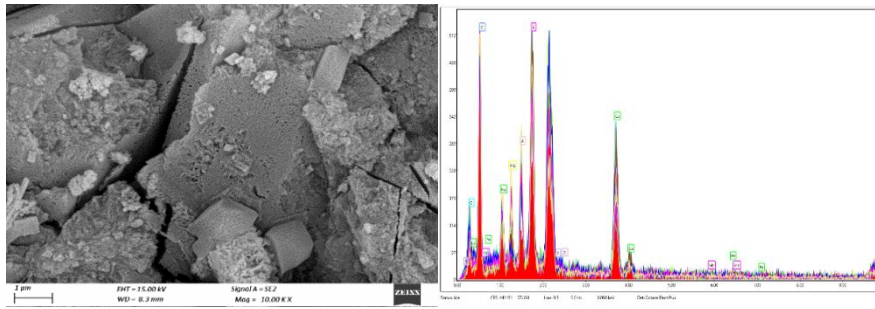
EDS was used to map composition and elemental composition, revealing Ca and Si as major elements, with moderate contributions from Na, Mg, and Al. Major elements influenced CSH gel formation, with Ca, Na, and Al responsible for CASH and NASH formation. Mg contributed to brucite, magnesite, magnesian calcite, and hydrotalcite formation. So far, the experimentally obtained molar ratios are shown in Table 4. The elemental ratios represent free ion concentrations in the pore solution, such as $[\text{Na}^+]$, $[\text{Al}^{+3}]$, $[\text{Si}^{+4}]$, $[\text{Mg}^{+2}]$, $[\text{Ca}^{+2}]$, $[\text{OH}^-]$, and so on. The elemental concentration decreases with age as the reaction progresses. Table 4 shows the EDX data for an average of 20 points. SF20NH10 has a lower Na concentration, indicating slower dissolution, and a higher $[\text{Al}^{+3}]$ concentration, indicating incomplete aluminosilicate dissolution. SF10NH10 shows a greater reduction in $[\text{Al}^{+3}]$ concentration at 28 days, indicating greater Al⁺³ ion engagement. Abdelrahman et al. (Abdelrahman and Garg, 2022) suggested that increasing the Na/Al ratio increased reaction speed until saturation was reached, but SF20NH8 showed a higher strength development (21.84% increase) for a lower increase in Na/Al ratio (52.48%). This extra strength is likely due to the coexistence of C-A-S-H and C-S-H, which are affected by decreasing Ca/Si ratio (Raúl Fernández et al., 2016). The strength of SF10NH10 was 35.1 MPa, with corresponding Na/Al increasing by 76.88% and Ca/Si decreasing by 43.12%, supporting the co-existence theory of the gels as reported in (Yip et al., 2005). The preceding statement was also supported by the formation of Tobermorite 14A in XRD, as well as Zeolite A and Zeolite X.

The Na/Ca ratio for SF10NH10 increased by 116% after 28 days, with additional Ca⁺² ions playing a crucial role in the formation of C-N-A-S-H and C-S-H. The presence of Mg⁺² in a Ca(OH)₂ or CaCO₃ system can result in the formation of magnesium-containing carbonate and the liberation of additional Ca⁺² ions (de Silva et al., 2009). The XRD showed brucite and magnesite at 7 and 28 days, proportional to the Mg/Ca ratio. Reactive MgO addition to GGBFS blends increases mechanical strength through hydrotalcite

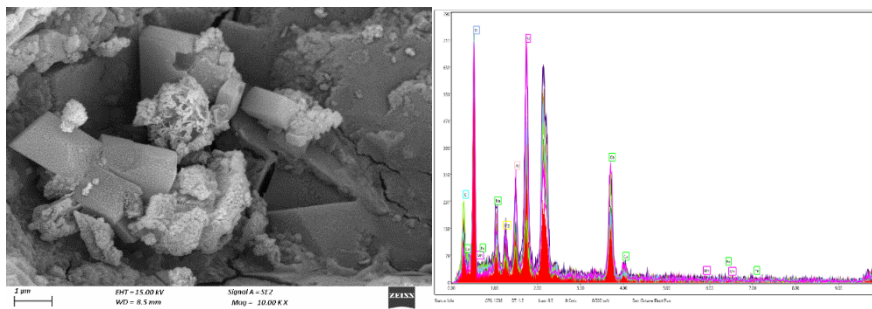
formation (Adeleke et al., 2021; Haha et al., 2011). The amount of freely available Mg significantly impacts the chemistry of the C-(N)-A-S-H gel (Walkley et al., 2017). The Mg/Al ratio ranged between 0.2 and 0.5 for all samples, confirming the lesser intensity of hydrotalcite (Kovtun et al., 2015; Wang and Scrivener, 1995). The presence of carbonates in a brucite sample can cause rapid formation of M-S-H phases, destabilizing it. This phenomenon is primarily observed when silica fume reacts with magnesium oxide or hydromagnesite in an environment rich in sodium carbonate (Barbara et al., 2018; Bernard et al., 2019; Monasterio-Guillot et al., 2021). However, the ratio in the current study was much lower, suggesting that this may not be the case. At room temperature, brucite in an alkaline medium can precipitate magnesium-calcite and/or (hydrated) magnesium carbonate (Montes-Hernandez et al., 2016). The decrease in calcite peaks and magnesite formation is accompanied by the formation of water molecules, resulting in SF10NH10 having higher strength despite having a higher amount of free water. At 28 days, the Mg/Ca for SF10NH10 increased, and the decrease in calcite peaks in XRD led to an 116% increase in the Na/Ca ratio. The presence of magnesian calcite in all samples also suggests this occurred.

Table 4: Experimental molar ratio of selected mixes

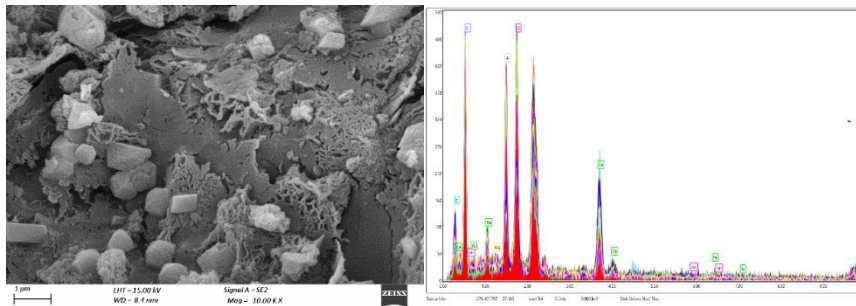
Mix	7 days									Compressive strength
	C	O	Na	Mg	Al	Si	Ca	Mn	Fe	
SF10NH8	4.72	23.00	4.48	3.14	8.40	24.31	26.66	1.52	1.62	25.93
SF20NH8	6.85	29.45	2.18	2.55	6.17	18.85	29.17	1.17	1.44	25.23
SF10NH10	4.52	26.39	4.36	0.29	12.39	20.22	29.00	1.37	1.89	29.97
SF20NH10	7.28	14.21	0.23	0.12	0.51	48.94	26.62	1.23	0.87	27.9
Mix	28 days									Compressive strength
	C	O	Na	Mg	Al	Si	Ca	Mn	Fe	
SF10NH8	13.56	21.46	4.64	2.43	7.01	18.41	16.76	12.87	0.11	29.76
SF20NH8	6.29	13.08	2.16	2.91	5.99	23.85	21.58	20.62	0.16	30.74
SF10NH10	19.07	16.16	5.53	3.63	7.93	20.87	17.03	15.71	0.15	35.1
SF20NH10	8.24	26.73	3.51	1.47	4.40	24.57	21.92	9.13	0.04	32.82



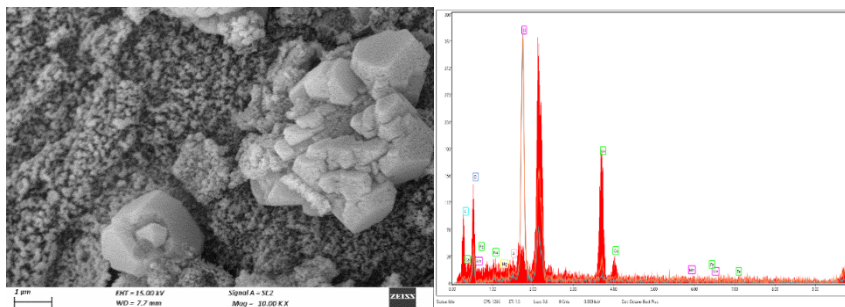
(a)



(b)

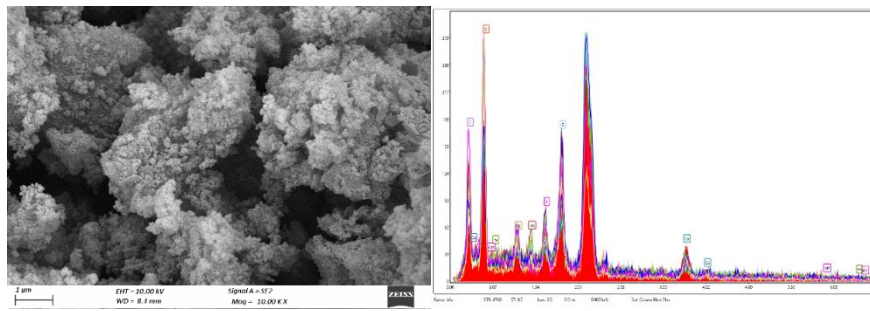


(c)

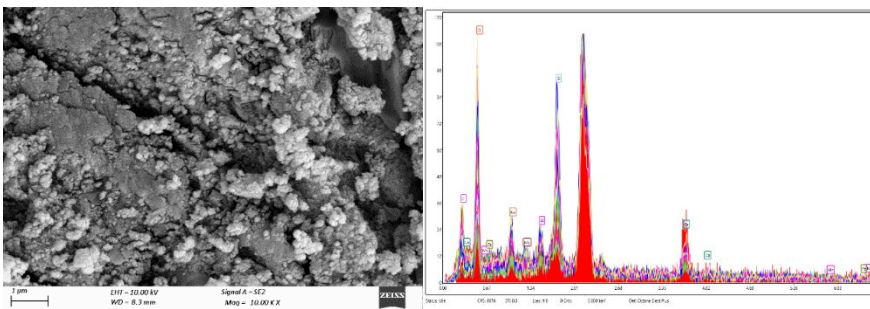


(d)

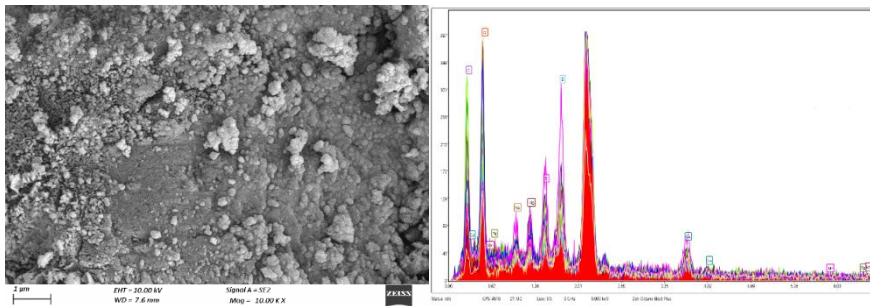
Figure 9: SEM images of mortar at 7 days containing (a) SF10NH8 (b) SF20NH8 (c) SF10NH10 (d) SF20NH10



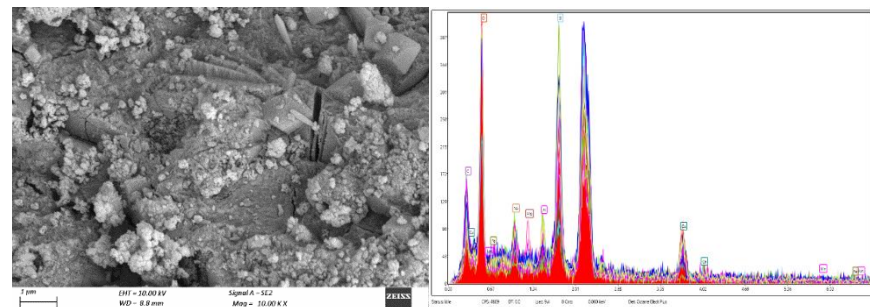
(a)



(b)



(c)



(d)

Figure 10: SEM images of mortar at 28 days containing (a) SF10NH8 (b) SF20NH8 (c) SF10NH10 (d) SF20NH10

4.5. Thermal Analysis

4.5.1. Phase Transitions

Figure 11 shows DTG thermograms of endothermic peaks of SF10NH8, SF20NH8, SF10NH10, and SF20NH10 at 28 days. Decomposition steps were grouped by temperature range, with 32°C to 105°C for water hydration, 105°C to 150°C for crystalline water removal, 150°C to 230°C for intra-layer water removal, 230°C to 420°C for gibbsite and brucite dehydroxylation, 420°C to 635°C for portlandite dehydroxylation, and 635°C to 800°C for calcite decomposition. The DTA thermogram confirmed phase transitions in the sample. The first endotherm was at A, indicating evaporation of free water, while the second endotherm was related to the breakdown of the thaumasite phase. A slight change in the slope at C indicated the start of polymeric gel decomposition, particularly C-A-S-H type gels, at 180°C. A prominent exotherm was observed beyond C, likely due to consecutive decomposition of the CSH and portlandite phases. The loss of inter-layer water of C-S-H started around 200°C, and $\text{Ca}(\text{OH})_2$ dehydroxylation occurred near 460°C via $\text{CaO} + \text{H}_2\text{O}$. The endothermic DTG peak at 435°C corresponded to oxidation and carbonation. An endothermic peak at E was attributed to the β - α quartz transformation in the sand. The characteristic amorphous profiles of C-S-H began to change from 615°-630°C, and an upward exotherm was observed at around 635°C due to crystallization. A simultaneous endotherm-exotherm was observed between 690°C and 715°C, likely due to magnesium calcite decomposing into magnesia, lime, and carbon dioxide.

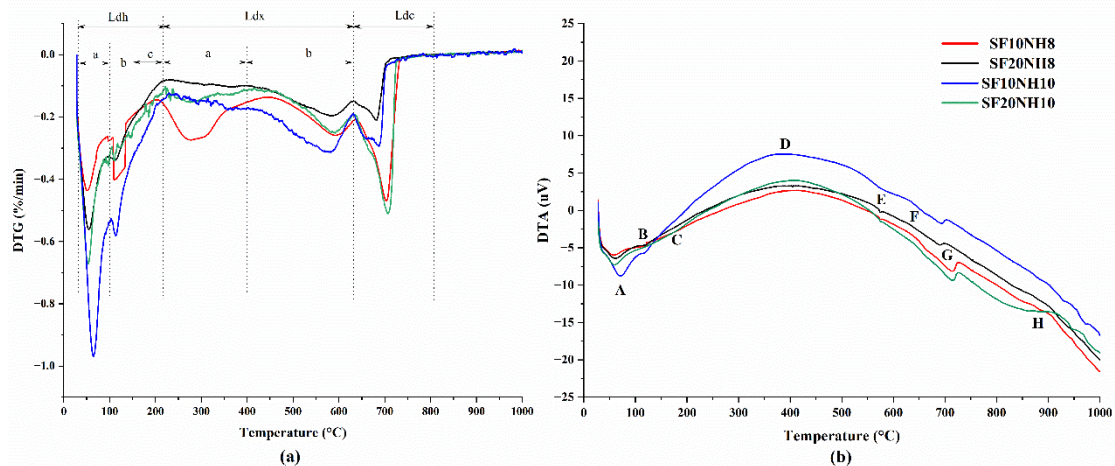


Figure 11: (a) DTG and (b) DTA curves of mortar at 28 days of SF10NH8, SF20NH8, SF10NH10, SF20NH10

4.5.2. Significance of TG-DTA Results

TG-DTA provided an indirect quantification of bound water in cementitious mixes (Bhatty, 1986; Deboucha et al., 2017; Monteagudo et al., 2014; Pane and Hansen, 2005), indicating gel formation. These study incorporated additive supplemented binders and incorporated mineral additives to calculate bound water. Bhatty's method (Bhatty, 1986) accounted for mass loss between 105°C and 1000°C, but did not account for carbonation due to anhydrous material in the presence of unreacted particles. Pane et al. (Pane and Hansen, 2005) corrected for anhydrous unreacted materials' additional carbonation. They did not, however, include the conversion factor for portlandite carbonation. Monteagudo's method (Monteagudo et al., 2014) combined both methods, resulting in a common expression for portlandite and anhydrous material. Deboucha (Deboucha et al., 2017) incorporated the mineral additive's influences via two major effects: filler and chemical effect, and mass drift. Deboucha's method is slightly modified in the resent study to estimate bound water associated with each chosen sample while taking additives' effects on hydration kinetics into account. Both Deboucha and Bessa (Bessa, 2004) stated that additive materials aided in hydration through the filler effect and chemical effect. Chemical activators in solid form aided in nucleation of precursor grains, but device drift was not considered due to negligible heating of the crucible.

$$W_B = Ldh + Ldx + 1.025(Ldc - Ldc_a) - (m_{precursor} \times LOI_{precursor} + m_{additive} \times (LOI_{SF} + LOI_{SA} + LOI_{HL})) \quad (10)$$

$$m_{precursor} = \frac{m_s - m_b \left(x_{SF} + x_{SA} + x_{HL} + \frac{W}{B} \right)}{1 + LOI_{precursor}} ;$$

$$m_{additive} = \frac{m_s - m_b \left(x_{GGBFS} + \frac{W}{B} \right)}{1 + LOI_{SF} + LOI_{SA} + LOI_{HL}}$$

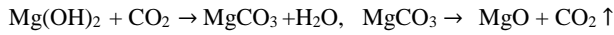
$m_s, m_b, x_{SF}, x_{SA}, x_{HL}, \frac{W}{B}, LOI_{SF}, LOI_{SA}, LOI_{HL}$ are the initial mass of the sample, and total binder mass, all considered as the equivalent of 1gm of sample, the replacement level of the additives (mineral and chemical), the water/binder ratio, and the loss on ignition of the additives (mineral and chemical) respectively. It was assumed that the activators completely react with water to initiate the dissolution.

The bound water was evaluated by estimating mass loss due to decarbonation of carbonated portlandite (Ldc-Ldc_a) and a portion of calcite from the initial ion exchange. The intensity reduction of calcite and the formation of additional magnesium calcite were determined from XRD and DTA readings. Magnesium was also included, with an

additional factor of 0.41. Magnesite formation was solely due to brucite carbonation, and magnesite decarbonation was accounted for by (Ldc-Ldc_a). A correction factor was required to account for both carbonated portlandite and calcite produced by ion exchange. The weight fraction of calcium carbonate (as balancing off the stoichiometry of the initial ion exchange) was subtracted from the total correction factor to directly evaluate the bound water associated with portlandite. The total correction factors are explained in equations (11-13) and the corrected bound water is evaluated in Table 12.



$$W_{B \text{ carbonated CH}} = \frac{W_{m\text{H}_2\text{O}}}{W_{m\text{CO}_2}} \times \text{Ldc} = 0.41 \text{ Ldc},$$



$$W_{B \text{ carbonated MH}} = \frac{W_{m\text{H}_2\text{O}}}{W_{m\text{CO}_2}} \times \text{Ldc} = 0.41 \text{ Ldc} \quad (12)$$



$$W_{B \text{ carbonated MH}} = \frac{W_{m\text{H}_2\text{O}}}{W_{m\text{CO}_2}} \times \text{Ldc} = \frac{0.41}{2} \text{ Ldc} = 0.205 \text{ Ldc} \quad (13)$$

Hence total correction factor is 1.025 (Ldc- Ldc_a).

Table 5: Weight of sample at different temperatures

Mix	W _{32°} (μg)	W _{105°} (μg)	W _{150°} (μg)	W _{230°} (μg)	W _{420°} (μg)	W _{635°} (μg)	W _{1000°} (μg)
SF10NH8	12866.57	12539.35	12364.07	12205.64	11715.84	11187.45	10825.05
SF20NH8	12454.08	12062.84	11910.97	11788.55	11576.26	11167.40	11037.15
SF10NH10	12408.41	11791.61	11544.55	11345.30	10998.91	10347.33	10137.07
SF20NH10	12547.22	12123.28	11967.29	11813.33	11518.06	11047.50	10671.72

Table 6: Evaluation of bound water content WB as per different studies

Mix	Free water Ldh _a (%)	Ldh (%)		Ldx (%)		LdC (%)	LdC _a (%)	Bound Water (%)
		Ldh _b	Ldh _c	Ldx _a	Ldx _b			
SF10NH8	2.543	1.398	1.264	3.906	4.214	2.890	1.898	10.578
SF20NH8	3.141	1.259	1.015	1.760	3.389	1.080	1.853	5.408
SF10NH10	4.971	2.095	1.690	2.938	5.526	1.783	2.038	10.783
SF20NH10	3.379	1.287	1.270	2.436	3.882	3.100	1.993	8.802

TG-DT analysis evaluates bound water and hydroxide phases, while free portlandite is

assessed using stoichiometry equations (11-13).

$$CH_{\text{free}} = \left(\frac{74.09}{18.01}\right) Ldx_b + \left(\frac{74.09}{44.01} - \%_{\text{calcite}}\right) (Ldc - Ldc_a) \quad (14)$$

where, $\left(\frac{74.09}{18.01}\right)$ is the molar mass ratio of Ca(OH)_2 to water, $\left(\frac{74.09}{44.01}\right)$ is the molar mass ratio of Ca(OH)_2 to CO_2 and $\%_{\text{calcite}}$ is the weight fraction of calcium carbonate as balanced off the stoichiometry of the initial ion exchange. Similarly, free gibbsite and free brucite could be evaluated as follows. To avoid overestimation, the weight fraction of calcium carbonate was subtracted in both assessments (Deboucha et al., 2017).

$$MH_{\text{free}} = \left(\frac{58.32}{18.01}\right) Ldx_a + \left(\frac{58.32}{44.01}\right) (Ldc - Ldc_a) \quad (15)$$

$$AH_{\text{free}} = \left(\frac{78}{18.01}\right) Ldx_a - MH_{\text{free}} \quad (16)$$

Table 12 shows corrected bound water and hydroxide estimations. SF10NH10 had the highest concentrations of bound water and hydroxides. 10% SF samples showed a significant improvement in strength gain, while NH10 samples showed higher strength gain. Higher MH ensured the formation of magnesium calcite and hydrotalcite (Montes-Hernandez et al., 2016), which increased strength. Higher AH in NH10 samples may indicate a higher pH, as the AH phase formation can be expressed as a function of pH (Zhang et al., 2021).

Table 7: Summary of CH, MH, AH, free water and bound water to corresponding strength

Mix	Free MH	Free AH	Free CH	Free Water	Bound Water	28-day Strength (MPa)	120-day Strength (MPa)	Increment in strength
SF10NH8	27.51	10.59	18.91	2.54	10.58	29.76	31.37	5.41
SF20NH8	15.73	8.11	12.72	3.14	5.41	30.74	31.57	2.70
SF10NH10	27.10	14.38	22.34	4.97	10.78	35.10	41.33	17.75
SF20NH10	21.78	11.24	17.69	3.38	8.80	32.82	39.17	19.35

5. Conclusions

To be deemed as a cost-effective binder material, industry grade soda ash and hydrated lime were investigated as solid activators in order to activate a silica fume blended slag mix. A “just add water” methodology was followed to meet the site requirements. The paste rheology and the strength development were observed; and the microstructural analysis and TGA-DTA study were done to validate the obtained results. Also, a side-by-side comparison with other mixing procedures was also done. Follow-up compressive

strength tests were also performed on control samples and pre-mixed soda ash samples.

The study brings out the following findings:

- (i) It can cost up to 60% more to use pre-mixed analytical grade Na_2CO_3 in water than to use a mixture that has been activated by NaOH pellets. Using industrial-grade chemicals, however, could reduce the price of the latter by 91%. It also saves 94.5 percent of the budget, when compared to analytical Na_2CO_3 counterparts.
- (ii) For a 10% SF addition and a 10% targeted NaOH content at a w/s ratio of 0.45, the mixes showed highest strength development and commendable rheology. The mix demonstrated 35.1 MPa after 28 days and 41.33 MPa after 120 days, making it suitable for use as a structural material. The corresponding initial strength for the control mix was low. At 28 days, the strength was comparable for mixes activated by a pre-mixed solution of NaOH (analytical grade). Mixes activated by a pre-mixed soda ash solution showed higher 28-day strength compared to the solid-state mixes. In all states, though, 10% SF and 10% NaOH showed the maximum strength development. However, the complementary analytical grade counterparts displayed greater strength at a lower activator percentage.
- (iii) Mixtures with NaOH solution as an activator displayed less yield stress. However, compared to an equivalent paste activated by solid soda ash and hydrated lime, the paste activated by pre-mixed soda ash solution showed noticeably higher yield stress.
- (iv) At 28 days, the XRD intensities of portlandite, calcite, and brucite were either reduced or disappeared. The presence of magnesian calcite, magnesite, and hydrotalcite was detected, which aided in strength gain by supplying Ca^{+2} for secondary reactions and the subsequent formation of CNASH; the presence of which was detected in the XRD of samples after 28 days of curing.
- (v) The SEM images show that, while CaCO_3 dominated the microstructure at 7 days, a denser microstructure developed at 28 days, which aided in the development of strength. Later-age samples were found to contain magnesian calcite as well as magnesite, according to EDS analysis. The TG-DT analysis also provided the same insights.
- (vi) TG-DT curves summarize phase transitions and bound water in hydration products; SF10NH10 exhibited higher strength due to calcite transitioning into magnesian calcite and portlandite.

Therefore, a practical substitute for analytical grade activators that provides high strength is dry direct mixing of industrial grade soda ash with the precursors. The final products are marginally different and helpful for increasing strength. Overall, this one-part mixture could function as a suitable, site-friendly binder. To design a concrete mix using the binder and investigate the performance-based properties, more research is required and is planned.

Disclosure Statement

The authors report there are no competing interests to declare.

References

- Abdalqader, A. F., Jin, F., & Al-Tabbaa, A. (2016). Development of greener alkali-activated cement: Utilisation of sodium carbonate for activating slag and fly ash mixtures. *Journal of Cleaner Production*, 113. <https://doi.org/10.1016/j.jclepro.2015.12.010>
- Abdelrahman, O., & Garg, N. (2022). Impact of Na/Al Ratio on the Extent of Alkali-Activation Reaction: Non-linearity and Diminishing Returns. *Frontiers in Chemistry*, 9. <https://doi.org/10.3389/fchem.2021.806532>
- Adeleke, B., Kinuthia, J., & Oti, J. (2021). Optimization of MgO-GGBS cementitious systems using thermo-chemical approaches. *Sustainability (Switzerland)*, 13(16). <https://doi.org/10.3390/su13169378>
- Adesina, A. (2020). Influence of various additives on the early age compressive strength of sodium carbonate activated slag composites: An overview. In *Journal of the Mechanical Behavior of Materials* (Vol. 29, Issue 1). <https://doi.org/10.1515/jmbm-2020-0011>
- Akturk, B., Nayak, S., Das, S., & Kizilkanat, A. B. (2019). Microstructure and Strength Development of Sodium Carbonate-Activated Blast Furnace Slags. *Journal of Materials in Civil Engineering*, 31(11). [https://doi.org/10.1061/\(ASCE\)MT.1943-5533.0002944](https://doi.org/10.1061/(ASCE)MT.1943-5533.0002944)
- Alonso, M. M., Gascó, C., Morales, M. M., Suárez-Navarro, J. A., Zamorano, M., & Puertas, F. (2019). Olive biomass ash as an alternative activator in geopolymer formation: A study of strength, durability, radiology and leaching behaviour. *Cement and Concrete Composites*, 104. <https://doi.org/10.1016/j.cemconcomp.2019.103384>
- Alonso, S., & Palomo, A. (2001). Alkaline activation of metakaolin and calcium hydroxide mixtures: Influence of temperature, activator concentration and solids ratio. *Materials Letters*, 47(1–2). [https://doi.org/10.1016/S0167-577X\(00\)00212-3](https://doi.org/10.1016/S0167-577X(00)00212-3)
- Alventosa, K. M. L., & White, C. E. (2021). The effects of calcium hydroxide and activator chemistry on alkali-activated metakaolin pastes. *Cement and Concrete Research*, 145. <https://doi.org/10.1016/j.cemconres.2021.106453>
- Athira, G., & Bahurudeen, A. (2022). Rheological properties of cement paste blended with sugarcane bagasse ash and rice straw ash. *Construction and Building Materials*, 332. <https://doi.org/10.1016/j.conbuildmat.2022.127377>
- Barbara, E. B., Daniel, L., Alexander, R., & Winnefeld, G. F. (2018). Effect of carbonates on the formation of magnesium silicate hydrates. *Materials and Structures*, 55. <https://doi.org/10.1617/s11527-022-02018-3>
- Bernal, S. A., Provis, J. L., Myers, R. J., San Nicolas, R., & van Deventer, J. S. J. (2014). Role of carbonates in the chemical evolution of sodium carbonate-activated slag binders. *Materials and Structures/Materiaux et Constructions*, 48(3). <https://doi.org/10.1617/s11527-014-0412-6>

- Bernard, E., Lothenbach, B., Pochard, I., & Cau-Dit-Coumes, C. (2019). Alkali binding by magnesium silicate hydrates. *Journal of the American Ceramic Society*, *102*(10). <https://doi.org/10.1111/jace.16494>
- Bessa, A. (2004). *Study of the contribution of mineral additions to the physical and mechanical durability of mortars*. University of Cergy-Pontoise, France.
- Bhatty, J. I. (1986). Hydration versus strength in a portland cement developed from domestic mineral wastes - a comparative study. *Thermochimica Acta*, *106*(C). [https://doi.org/10.1016/0040-6031\(86\)85120-6](https://doi.org/10.1016/0040-6031(86)85120-6)
- Calcium hydroxide CAS 1305-62-0 | 102047. (n.d.). Retrieved 31 March 2023, from https://www.merckmillipore.com/IN/en/product/Calcium-hydroxide,MDA_CHEM-102047
- Cheah, C. B., Tan, L. E., & Ramli, M. (2019). The engineering properties and microstructure of sodium carbonate activated fly ash/ slag blended mortars with silica fume. *Composites Part B: Engineering*, *160*. <https://doi.org/10.1016/j.compositesb.2018.12.056>
- Choo, H., Lim, S., Lee, W., & Lee, C. (2016). Compressive strength of one-part alkali activated fly ash using red mud as alkali supplier. *Construction and Building Materials*, *125*. <https://doi.org/10.1016/j.conbuildmat.2016.08.015>
- Deboucha, W., Leklou, N., Khelidj, A., & Oudjit, M. N. (2017). Hydration development of mineral additives blended cement using thermogravimetric analysis (TGA): Methodology of calculating the degree of hydration. *Construction and Building Materials*, *146*. <https://doi.org/10.1016/j.conbuildmat.2017.04.132>
- de Silva, P., Bucea, L., & Sirivivatnanon, V. (2009). Chemical, microstructural and strength development of calcium and magnesium carbonate binders. *Cement and Concrete Research*, *39*(5). <https://doi.org/10.1016/j.cemconres.2009.02.003>
- Flower, D. J. M., & Sanjayan, J. G. (2007). Green house gas emissions due to concrete manufacture. *The International Journal of Life Cycle Assessment*, *12*(5). <https://doi.org/10.1007/s11367-007-0327-3>
- Garcia-Lodeiro, I., Palomo, A., & Fernández-Jiménez, A. (2015). Crucial insights on the mix design of alkali-activated cement-based binders. In *Handbook of Alkali-Activated Cements, Mortars and Concretes*. <https://doi.org/10.1533/9781782422884.1.49>
- Haha, M. ben, Lothenbach, B., le Saout, G., & Winnefeld, F. (2011). Influence of slag chemistry on the hydration of alkali-activated blast-furnace slag - Part I: Effect of MgO. *Cement and Concrete Research*, *41*(9). <https://doi.org/10.1016/j.cemconres.2011.05.002>
- Handayani, L., Aprilia, S., Abdullah, Rahmawati, C., Aulia, T. B., Ludvig, P., & Ahmad, J. (2022). Sodium Silicate from Rice Husk Ash and Their Effects as Geopolymer Cement. *Polymers*, *14*(14), 2920. <https://doi.org/10.3390/polym14142920>
- Hardjito, D., & Rangan, B. V. (2005). Development and properties of low-calcium fly ash-based geopolymer concrete. In *Research report GC. hydrated lime - Shreeram Chemical Industries*. (n.d.). Retrieved 31 March 2023, from <https://www.indiamart.com/shreeramchemicalindustries/search.html?ss=hydrated+lime>
- Jackson, M. D., Mulcahy, S. R., Chen, H., Li, Y., Li, Q., Cappelletti, P., & Wenk, H. R. (2017). Phillipsite and Al-tobermorite mineral cements produced through low-temperature water-rock reactions in Roman marine concrete. *American Mineralogist*, *102*(7). <https://doi.org/10.2138/am-2017-5993CCBY>
- Jiao, Z., Wang, Y., Zheng, W., & Huang, W. (2018). Effect of dosage of sodium carbonate on the strength and drying shrinkage of sodium hydroxide based alkali-activated slag paste. *Construction and Building Materials*, *179*. <https://doi.org/10.1016/j.conbuildmat.2018.05.194>
- Kang, S. H., Kwon, Y. H., Hong, S. G., Chun, S., & Moon, J. (2019). Hydrated lime activation on byproducts for eco-friendly production of structural mortars. *Journal of Cleaner Production*, *231*. <https://doi.org/10.1016/j.jclepro.2019.05.313>
- Kearsley, E. P., Kovtun, M., & Shekhovtsova, J. (2015). Dry powder alkali-activated slag cements. *Advances in Cement Research*, *27*(8), 447–456. <https://doi.org/10.1680/adcr.14.00078>

- Kovtun, M., Kearsley, E. P., & Shekhovtsova, J. (2015). Chemical acceleration of a neutral granulated blast-furnace slag activated by sodium carbonate. *Cement and Concrete Research*, 72, 1–9. <https://doi.org/10.1016/j.cemconres.2015.02.014>
- Li, L., Ali, H. A., Lu, J. xin, & Poon, C. S. (2022). Role of silica fume in alkali-activated slag/glass powder paste. *Construction and Building Materials*, 356, 129189. <https://doi.org/10.1016/J.CONBUILDMAT.2022.129189>
- Li, Z., Zhang, S., Zuo, Y., Chen, W., & Ye, G. (2019). Chemical deformation of metakaolin based geopolymer. *Cement and Concrete Research*, 120. <https://doi.org/10.1016/j.cemconres.2019.03.017>
- Luukkonen, T., Abdollahnejad, Z., Yliniemi, J., Kinnunen, P., & Illikainen, M. (2018). One-part alkali-activated materials: A review. In *Cement and Concrete Research* (Vol. 103, pp. 21–34). Elsevier Ltd. <https://doi.org/10.1016/j.cemconres.2017.10.001>
- Ma, C., Zhao, B., Guo, S., Long, G., & Xie, Y. (2019). Properties and characterization of green one-part geopolymer activated by composite activators. *Journal of Cleaner Production*, 220, 188–199. <https://doi.org/10.1016/j.jclepro.2019.02.159>
- Monasterio-Guillot, L., Fernandez-Martinez, A., Ruiz-Agudo, E., & Rodriguez-Navarro, C. (2021). Carbonation of calcium-magnesium pyroxenes: Physical-chemical controls and effects of reaction-driven fracturing. *Geochimica et Cosmochimica Acta*, 304. <https://doi.org/10.1016/j.gca.2021.02.016>
- Monteagudo, S. M., Moragues, A., Gálvez, J. C., Casati, M. J., & Reyes, E. (2014). The degree of hydration assessment of blended cement pastes by differential thermal and thermogravimetric analysis. Morphological evolution of the solid phases. *Thermochimica Acta*, 592. <https://doi.org/10.1016/j.tca.2014.08.008>
- Montes-Hernandez, G., Findling, N., & Renard, F. (2016). Dissolution-precipitation reactions controlling fast formation of dolomite under hydrothermal conditions. *Applied Geochemistry*, 73. <https://doi.org/10.1016/j.apgeochem.2016.08.011>
- Moraes, J. C. B., Tashima, M. M., Akasaki, J. L., Melges, J. L. P., Monzó, J., Borrachero, M. V., Soriano, L., & Payá, J. (2017). Effect of sugar cane straw ash (SCSA) as solid precursor and the alkaline activator composition on alkali-activated binders based on blast furnace slag (BFS). *Construction and Building Materials*, 144. <https://doi.org/10.1016/j.conbuildmat.2017.03.166>
- Nežerka, V., Bílý, P., Hrbek, V., & Fládr, J. (2019). Impact of silica fume, fly ash, and metakaolin on the thickness and strength of the ITZ in concrete. *Cement and Concrete Composites*, 103. <https://doi.org/10.1016/j.cemconcomp.2019.05.012>
- Pane, I., & Hansen, W. (2005). Investigation of blended cement hydration by isothermal calorimetry and thermal analysis. *Cement and Concrete Research*, 35(6). <https://doi.org/10.1016/j.cemconres.2004.10.027>
- Price list for Soda Ash. (n.d.). Retrieved 31 March 2023, from <https://www.tatachemicals.com/price-list-for-soda-ash>
- Provis, J. L. (2018). Alkali-activated materials. In *Cement and Concrete Research* (Vol. 114, pp. 40–48). Elsevier Ltd. <https://doi.org/10.1016/j.cemconres.2017.02.009>
- Raúl Fernández, Ruiz, A. I., & Cuevas, J. (2016). Formation of C-A-S-H phases from the interaction between concrete or cement and bentonite. *Clay Minerals*, 51(2). <https://doi.org/10.1180/claymin.2016.051.2.09>
- Ren, J., Sun, H., Li, Q., Li, Z., Ling, L., Zhang, X., Wang, Y., & Xing, F. (2021). Experimental comparisons between one-part and normal (two-part) alkali-activated slag binders. *Construction and Building Materials*, 309. <https://doi.org/10.1016/J.CONBUILDMAT.2021.125177>
- Rostami, M., & Behfarnia, K. (2017). The effect of silica fume on durability of alkali activated slag concrete. *Construction and Building Materials*, 134. <https://doi.org/10.1016/j.conbuildmat.2016.12.072>
- Seymour, L. M., Tamura, N., Jackson, M. D., & Masic, A. (2022). Reactive binder and aggregate interfacial zones in the mortar of Tomb of Caecilia Metella concrete, 1C BCE, Rome. *Journal of the American Ceramic Society*, 105(2). <https://doi.org/10.1111/jace.18133>

- Shi, C., Jiménez, A. F., & Palomo, A. (2011). New cements for the 21st century: The pursuit of an alternative to Portland cement. In *Cement and Concrete Research* (Vol. 41, Issue 7, pp. 750–763). Elsevier Ltd. <https://doi.org/10.1016/j.cemconres.2011.03.016>
- Sodium carbonate CAS 497-19-8 | 106392. (n.d.). Retrieved 31 March 2023, from https://www.merckmillipore.com/IN/en/product/Sodium-carbonate,MDA_CHEM-106392
- Sodium hydroxide CAS 1310-73-2 | 106462. (n.d.). Retrieved 31 March 2023, from https://www.merckmillipore.com/IN/en/product/Sodium-hydroxide,MDA_CHEM-106462
- Teh, S. H., Wiedmann, T., Castel, A., & de Burgh, J. (2017). Hybrid life cycle assessment of greenhouse gas emissions from cement, concrete and geopolymer concrete in Australia. *Journal of Cleaner Production*, 152, 312–320. <https://doi.org/10.1016/J.JCLEPRO.2017.03.122>
- Vigneshwari, M., Arunachalam, K., & Angayarkanni, A. (2018). Replacement of silica fume with thermally treated rice husk ash in Reactive Powder Concrete. *Journal of Cleaner Production*, 188, 264–277. <https://doi.org/10.1016/j.jclepro.2018.04.008>
- Walkley, B., San Nicolas, R., Sani, M. A., Bernal, S. A., van Deventer, J. S. J., & Provis, J. L. (2017). Structural evolution of synthetic alkali-activated CaO-MgO-Na₂O-Al₂O₃-SiO₂ materials is influenced by Mg content. *Cement and Concrete Research*, 99, 155–171. <https://doi.org/10.1016/J.CEMCONRES.2017.05.006>
- Wang, J., Lyu, X. J., Wang, L., Cao, X., Liu, Q., & Zang, H. (2018). Influence of the combination of calcium oxide and sodium carbonate on the hydration reactivity of alkali-activated slag binders. *Journal of Cleaner Production*, 171. <https://doi.org/10.1016/j.jclepro.2017.10.077>
- Wang, S. D., & Scrivener, K. L. (1995). Hydration products of alkali activated slag cement. *Cement and Concrete Research*, 25(3). [https://doi.org/10.1016/0008-8846\(95\)00045-E](https://doi.org/10.1016/0008-8846(95)00045-E)
- Wu, M., Zhang, Y., Ji, Y., Liu, G., Liu, C., She, W., & Sun, W. (2018). Reducing environmental impacts and carbon emissions: Study of effects of superfine cement particles on blended cement containing high volume mineral admixtures. *Journal of Cleaner Production*, 196, 358–369. <https://doi.org/10.1016/J.JCLEPRO.2018.06.079>
- Yip, C. K., Lukey, G. C., & van Deventer, J. S. J. (2005). The coexistence of geopolymeric gel and calcium silicate hydrate at the early stage of alkaline activation. *Cement and Concrete Research*, 35(9). <https://doi.org/10.1016/j.cemconres.2004.10.042>
- Zhang, Y., Zhao, Q., Gao, Z., & Chang, J. (2021). Microstructure Control of AH3Gel Formed in Various Calcium Sulfoaluminate Cements as a Function of pH. *ACS Sustainable Chemistry and Engineering*, 9(34), 11534–11547. <https://doi.org/10.1021/acssuschemeng.1c03886>